

Research Paper

# Preliminary Therapy Evaluation of $^{225}\text{Ac}$ -DOTA-c(RGDyK) Demonstrates that Cerenkov Radiation Derived from $^{225}\text{Ac}$ Daughter Decay Can Be Detected by Optical Imaging for *In Vivo* Tumor Visualization

Darpan N. Pandya<sup>1</sup>, Roy Hantgan<sup>2</sup>, Mikalai M. Budzevich<sup>3</sup>, Nancy D. Kock<sup>4</sup>, David L. Morse<sup>5</sup>, Izadora Batista<sup>6</sup>, Akiva Mintz<sup>1,6,7</sup>, King C. Li<sup>7</sup>, Thaddeus J. Wadas<sup>1,7</sup> ✉

1. Department of Cancer Biology, Wake Forest School of Medicine, Winston-Salem, NC 27157 USA;
2. Department of Biochemistry, Wake Forest School of Medicine, Winston-Salem, NC 27157 USA;
3. Small Animal Imaging Laboratory, H. Lee Moffitt Cancer Center & Research Institute, Tampa, FL 33612 USA;
4. Department of Pathology-Section on Comparative Medicine, Wake Forest School of Medicine, Winston-Salem, NC 27157 USA;
5. Department of Cancer Imaging and Metabolism, H. Lee Moffitt Cancer Center & Research Institute, Tampa, FL 33612 USA;
6. Department of Neurosurgery, Wake Forest School of Medicine, Winston-Salem, NC 27157 USA;
7. Department of Radiology, Wake Forest School of Medicine, Winston-Salem, NC 27157 USA.

✉ Corresponding author: Thaddeus J. Wadas, Ph.D. Assistant Professor of Cancer Biology and Radiology, Wake Forest School of Medicine, Medical Center Blvd. Winston-Salem, NC 27157 phone: (336) 716-5696 fax: (336) 716-0255 e-mail: twadas@wakehealth.edu.

© Ivyspring International Publisher. Reproduction is permitted for personal, noncommercial use, provided that the article is in whole, unmodified, and properly cited. See <http://ivyspring.com/terms> for terms and conditions.

Received: 2015.01.27; Accepted: 2016.01.09; Published: 2016.03.01

## Abstract

The theranostic potential of  $^{225}\text{Ac}$ -based radiopharmaceuticals continues to increase as researchers seek innovative ways to harness the nuclear decay of this radioisotope for therapeutic and imaging applications. This communication describes the evaluation of  $^{225}\text{Ac}$ -DOTA-c(RGDyK) in both biodistribution and Cerenkov luminescence imaging (CLI) studies. Initially, La-DOTA-c(RGDyK) was prepared as a non-radioactive surrogate to evaluate methodologies that would contribute to an optimized radiochemical synthetic strategy and estimate the radioactive conjugate's affinity for  $\alpha_v\beta_3$ , using surface plasmon resonance spectroscopy. Surface plasmon resonance spectroscopy studies revealed the  $\text{IC}_{50}$  and  $K_i$  of La-DOTA-c(RGDyK) to be  $33 \pm 13$  nM and  $26 \pm 11$  nM, respectively, and suggest that the complexation of the  $\text{La}^{3+}$  ion to the conjugate did not significantly alter integrin binding. Furthermore, use of this surrogate allowed optimization of radiochemical synthesis strategies to prepare  $^{225}\text{Ac}$ -DOTA-c(RGDyK) with high radiochemical purity and specific activity similar to other  $^{225}\text{Ac}$ -based radiopharmaceuticals. This radiopharmaceutical was highly stable *in vitro*. *In vivo* biodistribution studies confirmed the radiotracer's ability to target  $\alpha_v\beta_3$  integrin with specificity; specificity was detected in tumor-bearing animals using Cerenkov luminescence imaging. Furthermore, tumor growth control was achieved using non-toxic doses of the radiopharmaceutical in U87mg tumor-bearing nude mice. To our knowledge, this is the first report to describe the CLI of  $\alpha_v\beta_3^+$  tumors in live animals using the daughter products derived from  $^{225}\text{Ac}$  decay *in situ*. This concept holds promise to further enhance development of targeted alpha particle therapy.

Key words: Actinium-225, Targeted Alpha Particle Therapy, Cerenkov Luminescence Imaging,  $\alpha_v\beta_3$  integrin.

## Introduction

The recent approval of Radium-223 ( $^{223}\text{Ra}$ ) by the United States Food and Drug Administration for palliative treatment of bone metastasis associated

with hormone-refractory prostate cancer has renewed interest in alpha particle ( $\alpha$ )-emitting radionuclides and targeted alpha particle therapy (TAT) [1-3]. This

type of therapy derives its efficacy from  $\alpha$ -particles, which are essentially helium (He) atom nuclei. Once ejected from the decaying nucleus, they travel less than 100 microns in a linear manner depositing a very large amount of energy through their path by ionization. This energy deposition, also referred to as Linear Energy Transfer (LET), is responsible for their enhanced cytotoxicity at activities far below those needed to achieve the same cell-killing efficiency of low LET  $\beta$ -emitters. Furthermore, when high-LET occurs within the cell nucleus irreparable double-stranded (ds) DNA breaks occur and result in activation of autophagy, necrosis, and cell cycle arrest pathways [4, 5]. Importantly,  $\alpha$ -particles do not rely on the generation of indirect reactive oxygen species; thus efficacy of TAT is not diminished by tumor hypoxia or chemoresistance that commonly develops after traditional chemotherapy. Finally, when properly targeted, the high LET of  $\alpha$ -particles can therapeutically target small clusters of malignant cells among normal tissues [2, 6-11].

Except for Radium-223 ( $^{223}\text{Ra}$ ), few  $\alpha$ -particle emitting radionuclides are used clinically due to incompatible half-lives, cost of production, and limited availability.  $^{225}\text{Ac}$  ( $t_{1/2} = 10$  d;  $E_{\alpha_{\text{max}}} = 6-8$  MeV) has gained considerable attention in TAT research because 1) it is readily available from Oak Ridge National Laboratories, 2) it has a 10-day half-life, 3) it functions as a nanogenerator at the tumor site, emitting 4  $\alpha$ -particles that release approximately 30 MeV of total kinetic energy per nuclear decay, 4) it can be chelated to DOTA, which is contained in numerous radiopharmaceuticals approved for clinical use or currently undergoing clinical trials, and 5) it is currently being used successfully in preclinical studies and clinical trials [2, 6-12]. Despite these attributes, biodistribution and pharmacokinetic data of  $^{225}\text{Ac}$ -based radiopharmaceuticals cannot be acquired using traditional pre-clinical imaging techniques such as positron emission tomography (PET) without significantly modifying the TAT radiopharmaceutical to accommodate a PET isotope. Although preclinical SPECT imaging with  $^{225}\text{Ac}$ -radiopharmaceuticals has been attempted through the detection of the 440 keV  $\gamma$  emission that occurs after  $^{213}\text{Bi}$  decay, data are limited since animals are typically euthanized 1 h after receiving the radiopharmaceutical and imaged 24 h after euthanasia to ensure isotopic equilibrium [13]. Thus, these experiments do not address the potential of longitudinal SPECT studies to inform development of  $^{225}\text{Ac}$ -radiopharmaceuticals. However, the ability to image and visualize  $^{225}\text{Ac}$ -based radiopharmaceutical biodistribution, metabolism, and clearance in animal models through longitudinal imaging studies would

be advantageous, since it is currently unavailable for preclinical stages of TAT development [14, 15].

The Cerenkov effect, observed nearly a half-century ago, describes the emission of ultraviolet light when certain charged particles exceed the phase velocity of light in a given medium [16, 17]. This effect can be observed using standard optical imaging systems originally designed to detect bioluminescence and fluorescence. Since first being described in molecular imaging research, the imaging and visualization of Cerenkov radiation, or Cerenkov luminescence imaging (CLI), has been demonstrated preclinically and clinically with various radioisotopes [16, 18]. Recently, several groups described the Cerenkov emissions derived from medically relevant isotopes, including  $^{225}\text{Ac}$ , which yields the largest optical signal among all isotopes examined [15, 19]. Since the  $\alpha$ -particle emitted during nuclear decay travels with low velocity, it was postulated that the observed emission resulted from the beta decay of  $^{213}\text{Bi}$ ,  $^{209}\text{Tl}$ , and  $^{209}\text{Pb}$  in the  $^{225}\text{Ac}$  decay chain. Subsequent reports using theoretical and experimental means described the association between Cerenkov radiation and  $^{225}\text{Ac}$  decay, but did not use an  $^{225}\text{Ac}$ -based radiopharmaceutical in an animal model to demonstrate its applicability to drug or radiopharmaceutical development [19, 20]. In this communication, we provide initial evidence that the secular equilibrium between  $^{225}\text{Ac}$  and its daughter products can be harnessed to visualize TAT delivery in live animals, using standard optical imaging techniques. We accomplished this by synthesizing  $^{225}\text{Ac}$ -DOTA-c(RGDyK) and evaluating its stability, biodistribution, and potential use as an imaging agent in CLI in a murine model expressing human glioblastoma U87mg tumors, which overexpress the  $\alpha_v\beta_3$  integrin. This receptor is a member of the integrin superfamily and is overexpressed in malignancies and on neovasculature necessary for tumor growth [21, 22]. Finally, preliminary toxicity and therapy studies were conducted to demonstrate the effect of  $^{225}\text{Ac}$ -DOTA-c(RGDyK) on tumor growth, to further assess the theranostic potential of this approach.

## Materials and Methods

Unless otherwise noted, all chemicals were purchased from Sigma-Aldrich Chemical Co. (St. Louis, MO, USA), and solutions were prepared using ultrapure water (18 M $\Omega$ -cm resistivity). DOTA-c(RGDyK) was purchased from CPC Scientific, Inc. (Sunnyvale, CA), and its purity and mass were confirmed at Wake Forest using HPLC and electrospray ionization (ESI) mass spectrometry as described below. Recombinant human  $\alpha_v\beta_3$  integrin was purchased from R&D Systems, Inc. (Minneapolis,

MN). Cyclo-L-Arg-Gly-L-Asp-D-Tyr-L-Lys (cRGDyK) was purchased from AnaSpec (Freemont, CA).  $^{225}\text{Ac}(\text{NO}_3)_3$  ( $t_{1/2} = 10$  d;  $E_{\alpha_{\text{max}}} = 6\text{--}8$  MeV) was received from Oak Ridge National Laboratory (Oak Ridge, TN) and dissolved in 0.2 M Optima grade hydrochloric acid (HCl, Fisher Scientific) before use. Electrospray ionization (ESI) mass spectra were obtained on an Agilent 1100 LC/MSD in the Wake Forest University Department of Chemistry.

The radiochemistry reaction progress and purity were analyzed using a Waters analytical HPLC (Milford, MA), which runs Empower software and is configured with a 1525 binary pump, 2707 autosampler, 2998 photodiode array detector, 2475 multichannel fluorescence detector, 1500 column heater, fraction collector, Grace Vydac 218MS C18 column (5  $\mu\text{m}$ , 4.6  $\times$  250 mm, Grace Davidson, Deerfield, IL) and a Carrol Ramsey 105-s radioactivity detector (Berkeley, CA). DOTA-c(RGDyK) and the associated La-DOTA-c(RGDyK) complex were monitored at 220 nm using a mobile phase consisting of 0.1% TFA/ $\text{H}_2\text{O}$  (solvent A) and 0.1% TFA/acetonitrile (solvent B), and a gradient consisting of 0% B to 70% B in 20 min at a flow rate of 1.2 mL/min. In addition, radio-TLC was conducted on a Bioscan AR 2000 radio-TLC scanner equipped with a 10% methane:argon gas supply and a PC interface running Winscan v.3 analysis software (Eckert & Ziegler, Berlin, DE). Varian ITLC-SG strips and Merck C18 TLC plates were employed using a 0.9% NaCl/10 mM NaOH and 30:70 10%  $\text{NH}_4\text{OAc}$ /methanol solution as eluents, and  $^{225}\text{Ac}(\text{NO}_3)_3$  as a standard control. Activity of radioactive samples was measured using previously described procedures with either a CRC-25R radioisotope calibrator (Capintec, Inc.) or a Perkin Elmer 2480 Wizard<sup>®</sup> gamma counter (Waltham, MA) [23].

### Synthesis of La-DOTA-c(RGDyK)

A 1.5 mL vial was charged with DOTA-c(RGDyK) (200  $\mu\text{g}$ , 0.17  $\mu\text{mol}$ ),  $\text{LaCl}_3$  (76.1  $\mu\text{g}$ , 0.20  $\mu\text{mol}$ ), 0.2 mL of water, and 6  $\mu\text{L}$  0.1 M  $\text{Na}_2\text{CO}_3$ . The pH of the resulting solution was 5.5–6, and it was stirred for 1 h at 70 °C. The product was obtained in quantitative yield and lyophilized to a white solid. Formation of La-DOTA-c(RGDyK) was confirmed by ESI-MS analysis. Calculated for  $\text{C}_{51}\text{H}_{72}\text{N}_{14}\text{O}_{16}\text{SLa}$ , 1307.4 [(M+2H)<sup>+</sup>] Observed: 1307.6 [(M+2H)<sup>+</sup>].

### Radiochemical synthesis of $^{225}\text{Ac}$ -DOTA-c(RGDyK), Quality Control, and *in vitro* Serum Stability

The complexation of  $^{225}\text{Ac}$  with DOTA-c(RGDyK) was achieved by reacting DOTA-

c(RGDyK) (5–10  $\mu\text{g}$  (5–10  $\mu\text{L}$ , 1.0 mg/mL in water)) with  $^{225}\text{Ac}(\text{NO}_3)_3$  (3.4 MBq) that was diluted in 100  $\mu\text{L}$  of water containing 10  $\mu\text{L}$  of 20% L-ascorbic acid. The pH of the resulting solution was adjusted to 5.5–6 using 1 M Tris buffer (10–12  $\mu\text{L}$ ), and then incubated at 60 °C for 1 h. Reaction progress and radiochemical purity of  $^{225}\text{Ac}$ -DOTA-c(RGDyK) were measured without further purification using ITLC with gamma counting, radio-TLC, gamma counting of radio-HPLC fractions, or CLI. *In vitro* serum stability was carried out by adding 50  $\mu\text{L}$  of  $^{225}\text{Ac}$ -DOTA-c(RGDyK) (2 MBq) to 900  $\mu\text{L}$  of human serum. The solutions ( $n = 4$ ) were incubated at 37 °C for 10 days and were analyzed daily using radio-TLC, ITLC with gamma counting or size exclusion chromatography using a Superdex 200 10/300 GL<sup>™</sup> column (GE Healthcare Life Sciences, Piscataway, NJ) and phosphate buffered saline (PBS) as eluent with a flow rate of 0.5 mL/min.

### Surface Plasmon Resonance Spectroscopy (SPR) of La-DOTA-c(RGDyK)

Lyophilized samples stored at -20 °C were reconstituted to 100  $\mu\text{g}/\text{mL}$  in 130 mM NaCl, 10 mM HEPES, 1 mM  $\text{CaCl}_2$ , 1 mM  $\text{MgCl}_2$ , pH 7.4 (HBS) for SPR measurements. Samples of the lyophilized peptide were dissolved in water (5 mg/mL) and then diluted in sodium acetate buffer (50  $\mu\text{g}/\text{mL}$ ; pH 5.0) for coupling to biosensor chips. CM-5 biosensor chips (Biacore, Inc., Piscataway, NJ) were activated for amine coupling by reaction with 1-ethyl-3-(3-dimethylaminopropyl) carbodiimide and N-hydroxysuccinimide in a Biacore T100 instrument [24, 25]. c(RGDyK) (50  $\mu\text{g}/\text{mL}$ ) in 0.1 M sodium acetate buffer (pH 5.0) was delivered to the sample chamber, yielding immobilization densities of 222 response units (RU) for the  $\alpha_v\beta_3$ :c(RGDyK) binding series and 196 RU for the La-DOTA-c(RGDyK) competition series. Residual active groups were blocked with ethanolamine. Interactions between immobilized c(RGDyK) and recombinant human integrin and La-DOTA-c(RGDyK) were measured by collecting the signals from both reference and sample channels at 10 Hz. Reagents were maintained at  $25.0 \pm 0.1^\circ\text{C}$  in the sample compartment; experiments were performed at  $25.00 \pm 0.01^\circ\text{C}$  in the analysis chamber. Two start-up cycles were performed in which HEPES buffered saline (HBS) was delivered, followed by a 2-step regeneration cycle (20 mM EDTA in HBS for 180 sec then 5 M NaCl in water for 180 sec). During the binding steps, increasing concentrations (0 – 300 nM) of  $\alpha_v\beta_3$  in HBS were delivered at 30  $\mu\text{L}/\text{min}$  for 1000 sec. Dissociation of the  $\alpha_v\beta_3$  integrin:ligand complex was monitored for 1000 sec, as HBS flowed over the biosensor surface at 30  $\mu\text{L}/\text{min}$ , and residual bound integrin was displaced by the regeneration

cycle. The biosensor was then equilibrated for 300 sec with HBS before delivery of the next integrin aliquot. Sensorgram data (sample - reference signals) were further corrected by subtracting the time-dependent profiles obtained with a buffer blank. These doubly corrected signals were then fit globally by nonlinear regression (Biacore Evaluation software); first to a single-site binding model, and then to a ligand-induced conformational change model [25, 26]. In each case, the quality of the fit was judged by the residuals and the reduced  $\chi^2$  value. For competition experiments, the  $\alpha_v\beta_3$  concentration was fixed at 83 nM and samples containing increasing concentrations of La-DOTA-c(RGDyK) were prepared for delivery to immobilized c(RGDyK) (*vide supra*).

### Animal Models

All animal experiments were conducted in compliance with Institutional Animal Care and Use Committee guidelines established by Wake Forest University Health Sciences. Normal BALB/c and nude mice (weight, 20–22 g; age, 6–8 wk) were purchased from Jackson Laboratories (Bar Harbor, ME). Thirty-six female athymic nu/nu mice were subcutaneously injected into the flank with U87mg human glioblastoma tumor cells ( $1 \times 10^6$  cells; ATCC, Inc., Manassas, VA). Cell growth was evaluated weekly using a manually measured tumor volume (volume =  $0.52 \times [\text{width}]^2 \times [\text{length}]$ ) until tumors reached a palpable mass.

### Biodistribution and Dosimetry of $^{225}\text{Ac-DOTA-c(RGDyK)}$

Biodistribution studies were conducted as previously described [27]. Briefly, tumor-bearing mice ( $n = 6/\text{time point}$ ) were injected with  $^{225}\text{Ac-DOTA-c(RGDyK)}$  (0.7 MBq, 40 ng in 150  $\mu\text{L}/\text{mouse}$ ) via the tail vein. Blocking studies were also performed to examine *in vivo* uptake and specificity. Animals received a co-injection of c(RGDyK) (500 fold molar excess) along with  $^{225}\text{Ac-DOTA-c(RGDyK)}$ . Animals were sacrificed at 1, 4 and 24 h post-injection (p.i.) and organs of interest were removed, weighed, and subjected to gamma counting 24 hours after sacrifice. The percent injected dose per gram (%ID/g) and percent injected dose per organ (%ID/organ) were calculated by comparison to a weighed, counted standard.

Dosimetry was estimated as previously described [28]. Briefly, the amount of gamma radioactivity in the tumor and kidney was measured using gamma counting. The gamma-ray lines of  $^{225}\text{Ac}$  corresponding to the amount of alpha radioactivity was calculated according to known procedures [29], and time-activity curves were generated. Integration

of the data followed by the application of standard medical internal radiation dose methods for alpha particles yielded the absorbed dose  $D$  (rad) and average dose equivalent  $H$  (Sv) per organ [30].

### Small Animal Optical Imaging using Cerenkov Luminescence

Imaging studies were conducted using a modified procedure [15]. Briefly, all tumor-bearing mice ( $n = 6/\text{cohort}$ ) received an injection of  $^{225}\text{Ac-DOTA-c(RGDyK)}$  (1.9 MBq, 40 ng in 150  $\mu\text{L}/\text{mouse}$ ) via the tail vein. Blocking studies were also performed at 24 h. Animals received a co-injection of c(RGDyK) (500 fold molar excess) along with  $^{225}\text{Ac-DOTA-c(RGDyK)}$ . Mice were anesthetized with 1–2% isoflurane and imaged at 24 h p.i. After the 24 h time point, animals were euthanized and tumors and organs of interest were removed and imaged *ex vivo*. Optical images were collected using a Xenogen IVIS 100 optical imager (f/stop: 2; binning 1, field of view B) with no light interference from the excitation lamp. Images were analyzed using the Living Image 2.6 software (Caliper Life Sciences, Alameda, CA). The average radiance ( $\text{p/s}/\text{cm}^2/\text{sr}$ ) was used for quantitative region of interest (ROI) analysis from each image. Background correction was performed through (a) use of dark images acquired at the equivalent instrument integration setting immediately before experimental image collection, or (b) ROI analysis of a region in the same experimental image but remote from the area of interest.

### Therapy Studies

Maximum tolerated dose studies (MTD) were conducted using eight cohorts of normal BALB/c mice. After a single intravenous injection of  $^{225}\text{Ac-DOTA-c(RGDyK)}$  or saline, cohorts ( $n = 5$  mice/cohort) were weighed 3 times/week, and monitored for 110 days for signs of distressed behavior. At the end of that period, animals were euthanized and serum was collected. Blood urea nitrogen (BUN) and creatinine content in serum was analyzed using commercial ELISA kits (Biotrend Chemikalien GmbH, Germany). Heart, lung, liver, kidney, spleen, pancreas, stomach, small intestine, large intestine, muscle and bone were harvested, fixed in 10% formalin, embedded in paraffin, sectioned (4–6  $\mu\text{m}$  thickness), stained with hematoxylin and eosin, and examined. Weight, serum and pathology data were correlated to determine the MTD.

Four days before radiotherapy administration, female nude mice were inoculated in the flank with U87 mg cells, and then randomly divided into cohorts ( $n = 10/\text{cohort}$ ). Each cohort received a single intravenous injection of either saline, DOTA-

c(RGDyK) or  $^{225}\text{Ac}$ -DOTA-c(RGDyK). Doses were determined from the results of the MTD study. Animals were monitored daily for signs of distressed behavior, and tumor growth was evaluated thrice weekly using manual tumor volume (volume =  $0.52 \times [\text{width}]^2 \times [\text{length}]$ ) measurements. Mice were sacrificed 18 days after tumor cell inoculation as previously described [31].

### Statistical Methods

All data are presented as mean $\pm$ SD or mean (95% confidence intervals). For statistical classification, Student's t test (two-tailed, unpaired) was performed either using Prism 6.0 (GraphPad Software, Inc., San Diego, CA) or SigmaPlot (Systat Software, Inc. San Jose, CA). For therapy data, a one-way ANOVA test (including Dunnett's multiple comparison test) was performed. A  $p < 0.05$  was considered significant.

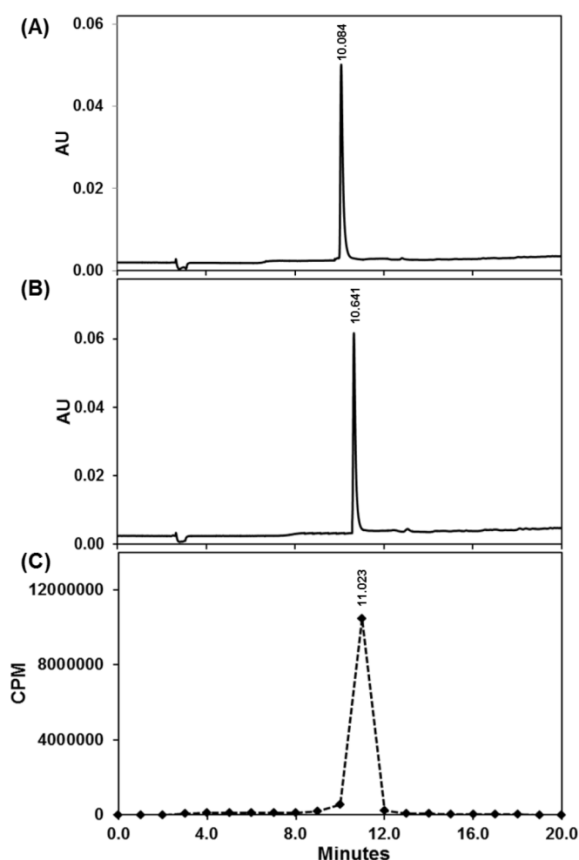


**Figure 1. Quality control of  $^{225}\text{Ac}$ -DOTA-c(RGDyK) using Radio-HPLC.** UV-HPLC chromatogram (220 nm) of DOTA-c(RGDyK) (A) and nonradioactive La-DOTA-c(RGDyK) (B) compared with radio-HPLC chromatogram of  $^{225}\text{Ac}$ -DOTA-c(RGDyK) (C).

## Results and Discussion

The reliable availability of carrier-free  $^{225}\text{Ac}$  from Oak Ridge National Laboratories or The Institute of Transuranium Elements has allowed the theranostic potential of  $^{225}\text{Ac}$  to be tested [2, 9]. However, unlike

many radionuclides used in imaging and therapy, the high cost of actinium and the lack of stable isotopes to facilitate even the most basic studies for ligand development or conjugate performance at an early preclinical stage have retarded progress. To facilitate our studies in development of  $^{225}\text{Ac}$ -DOTA-c(RGDyK), we chose to prepare La-DOTA-c(RGDyK) as a non-radioactive surrogate to develop an initial synthetic route to the  $^{225}\text{Ac}$ -radiopharmaceutical and evaluate the conjugate's affinity for  $\alpha_v\beta_3$  integrin once the trivalent ion was chelated to the conjugate (see **Scheme S1** of the Supporting Information (SI)). We hypothesized that the use of  $\text{La}^{3+}$  was appropriate, since the reaction conditions needed to prepare many  $^{225}\text{Ac}$  compounds or complexes parallel those used to synthesize analogous  $\text{La}^{3+}$  compounds and complexes. Since their chemistries are highly similar in both preparative and analytical experiments,  $\text{La}^{3+}$  is considered a useful surrogate for  $^{225}\text{Ac}^{3+}$  [32, 33]. Accordingly, we prepared La-DOTA-c(RGDyK) in quantitative yield using a modified literature procedure [34], and confirmed the identity of this complex using analytical HPLC (**Figure 1**) and electrospray ionization mass spectrometry (ESI<sup>+</sup>-MS) (**Figure S1**).

We then determined the affinity of this conjugate for  $\alpha_v\beta_3$  using SPR, a sensitive optical technique that provides real-time kinetic data for binding a receptor (delivered in solution by microfluidics) to a ligand (immobilized on a biosensor) [35, 36]. This powerful analytical tool has many applications in environmental protection, biotechnology, medical diagnostics, and drug discovery [37]. Initially, we sought to determine the rate, affinity, and specificity of the interactions between  $\alpha_v\beta_3$  and c(RGDyK). Increasing concentrations of  $\alpha_v\beta_3$  were delivered to a biosensor derivatized with c(RGDyK). SPR data showed time- and concentration-dependent increases in RU when  $\alpha_v\beta_3$  interacted with c(RGDyK) (**Figure S2**). RU signals were reduced to near-background values when c(RGDyK) was included at 11- and 115-fold molar excess over  $\alpha_v\beta_3$  (30 nM). These competition results demonstrate that our SPR approach reports specific  $\alpha_v\beta_3$ :c(RGDyK) binding [24]. The  $\alpha_v\beta_3$  binding data (10 concentrations ranging from 3 - 300 nM) were fit to a reversible two-state bimolecular interaction model, to determine the forward ( $k_{a1}$ , L/mol-sec) and reverse ( $k_{d1}$ , sec<sup>-1</sup>) rate constants for the initial binding step and forward ( $k_{a1}$ , sec<sup>-1</sup>) and reverse ( $k_{d2}$ , sec<sup>-1</sup>) rate constants for the subsequent stabilizing conformational change (**Figure S2**) [25]. The quality of the fit can be judged by the close correspondence between the solid lines and the data in **Figure S3** and the tightly distributed residuals. This data set yielded  $k_{a1}$  of  $1.58 \pm 0.01 \times 10^4$  L/mol-sec

and a  $k_{d1}$  of  $9.91 \pm 0.03 \times 10^{-3} \text{ sec}^{-1}$  at 25 °C. These studies also revealed the kinetic parameters for the conformational change step ( $k_{a2}$  of  $1.22 \pm 0.01 \times 10^{-3} \text{ sec}^{-1}$  and  $k_{d2}$  of  $1.23 \pm 0.01 \times 10^{-3} \text{ sec}^{-1}$ ; **Figure S2**). The overall  $K_d$  for the reaction was  $3.16 \times 10^{-7} \text{ mol/L}$ . Attempts to fit the  $\alpha_v\beta_3:c(\text{RGDyK})$  binding data to a single-site kinetic model proved problematic, yielding large deviations between the biphasic association and dissociation profiles and the fitted lines [26, 35, 36, 38]. Recognizing that binding RGD ligands perturb  $\alpha_v\beta_3$  resting conformation, we focused on a ligand-induced conformational change model that others have successfully applied to analyze multiphasic SPR kinetic data [39-44].

Our next goal was to determine how tightly  $\alpha_v\beta_3$  binds La-DOTA-c(RGDyK). However, amine coupling of this conjugate to a biosensor chip was precluded because its lysine residue was blocked by derivatization. Hence, we followed a competition approach in which  $\alpha_v\beta_3$  (83 nM) binding to immobilized c(RGDyK) was first measured, followed by two samples with increasing concentrations of La-DOTA-c(RGDyK) [26]. This three-step sequence was followed to examine competitor concentrations of 9, 26, 94, 300, 915, 2515, 10061, 37729 nM, covering a range of 0.1 – 450-fold molar excess. The resultant kinetic traces (**Figure S4**) show a concentration-dependent decrease in  $\alpha_v\beta_3$  binding signals (RU), which approached baseline values as the concentration of La-DOTA-c(RGDyK) approached 300 nM. Plotting RU vs La-DOTA-c(RGDyK) molar excess over  $\alpha_v\beta_3$  (log scale) yielded a sigmoid profile characterized by an  $\text{IC}_{50}$  equivalent to  $0.40 \pm 0.16$  fold-molar excess [26]. This corresponds to an  $\text{IC}_{50}$  of  $33 \pm 13 \text{ nM}$  and yields a  $K_i$  of  $26 \pm 11 \text{ nM}$ , which align with literature reports describing  $^{68}\text{Ga}$ - or  $^{64}\text{Cu}$ -RGD based radiopharmaceuticals [45, 46]. Furthermore, the similarity of our results with published values for DOTA-c(RGDyK) implies that complexation of the  $\text{La}^{3+}$  ion by the conjugate does not interfere with integrin binding and suggests that efficient binding of  $^{225}\text{Ac}$ -DOTA-c(RGDyK) to  $\alpha_v\beta_3$  is likely to occur *in vivo*.

Based on our synthetic strategy to prepare La-DOTA-c(RGDyK), we prepared  $^{225}\text{Ac}$ -DOTA-c(RGDyK) with a radiochemical purity greater than 99.8%, a radiochemical yield greater than 95%, and specific activity of 680 kBq/ $\mu\text{g}$  (**Scheme S2**). These values are based upon results obtained from ITLC in conjunction with gamma counting that revealed a single radiolabeled product, which eluted with the solvent front. Although few  $^{225}\text{Ac}$ -labeled peptides have been reported, the specific activity for our tracer is well within the spectrum reported for similar radiopharmaceuticals [31, 47]. Additionally, we

sought to determine if  $^{225}\text{Ac}$ -radiopharmaceuticals could be analyzed using radio-TLC, HPLC with gamma counting or CLI, since their use in this arena has not been reported previously (**Figure 1** and **S5**). Although ITLC has been used traditionally for  $^{225}\text{Ac}$  radiopharmaceutical purity determination, all these techniques can be informative during radiopharmaceutical synthesis and may enhance development of TAT. We obtained quality control samples and then waited 24 hours so that the secular equilibrium between  $^{225}\text{Ac}$  and its daughter products was established. Based on radio-TLC analyses, we observed that unchelated  $^{225}\text{Ac}$  remained at the origin ( $R_f = 0$ ), whereas  $^{225}\text{Ac}$ -DOTA-c(RGDyK) eluted near the solvent front ( $R_f = 0.86$ ). Additionally, CLI of the same TLC plates indicated only one spot at the origin and one near the solvent front (**Figure S5**). Although CLI resolution is poor compared to that of the radio-TLC scanner, two samples with significantly different  $R_f$  values could be distinguished; thereby providing qualitative confirmation of the radio-TLC results in excellent agreement with our ITLC data. Further corroboration of purity was provided by measuring radioactivity in HPLC fractions, which was determined by gamma counting using a 190-230 keV window. Plotting the results per unit time demonstrated we synthesized  $^{225}\text{Ac}$ -DOTA-c(RGDyK) in 99.8% purity, which agreed with the gamma counting results from ITLC plates. Using this technique,  $^{225}\text{Ac}$ -DOTA-c(RGDyK) had a retention time of 11.02 minutes, similar to the UV-HPLC chromatograms of DOTA-c(RGDyK) and the non-radioactive analogue, La-DOTA-c(RGDyK) (**Figure 1**).

For initial stability studies, we incubated  $^{225}\text{Ac}$ -DOTA-c(RGDyK) in an aliquot of human serum for 10 days at physiological temperature (see **Table S1** for results). After 10 days, less than 5% of the radiopharmaceutical had degraded in the presence of serum proteins. We observed similar results when analyzing samples using radio-TLC or ITLC with traditional gamma counting, suggesting that these techniques can accurately describe the stability of  $^{225}\text{Ac}$  radiopharmaceuticals. However, since daughter nuclei could be bound to serum proteins that do not migrate in our ITLC system, we elected to perform size exclusion chromatography to further characterize the stability of our radiotracer and the results of these experiments are depicted in **Figure S6**. When samples of serum which contained unchelated  $^{225}\text{Ac}$  were analyzed using SE chromatography, we observed a large peak, whose elution started at 28 minutes and ended at 38 minutes. The peak patterns and elution profile matched that of serum protein components, which were observed in the UV chromatogram at 220

nm. In contrast, in serum samples containing the radiotracer, a minor peak (5%) was observed at 30 minutes, which correlated with serum proteins in the UV profile; the major peak (95%) eluted between 41-45 minutes and might reflect the intact radiopharmaceutical, which further corroborates the stability results obtained using ITLC and radio-TLC. While few  $^{225}\text{Ac}$ -peptide based radiopharmaceuticals are available for comparison,  $^{225}\text{Ac}$ -DOTA conjugated antibodies demonstrate similar stabilities in human serum, and further reinforce the observed stability of  $^{225}\text{Ac}$ -DOTA-c(RGDyK) *in vitro* [48, 49].

We evaluated  $^{225}\text{Ac}$ -DOTA-c(RGDyK), by conducting biodistribution studies in  $\alpha_v\beta_3^+$  U87mg tumor bearing mice, since U87mg tumor cells overexpress  $\alpha_v\beta_3$  integrin. This model was used successfully in previous studies to evaluate several PET and SPECT radiopharmaceuticals designed to image  $\alpha_v\beta_3$  expression [46].  $^{225}\text{Ac}$ -DOTA-c(RGDyK) showed rapid blood clearance, with 99% of the activity present at 1 h removed from the blood by 24 h (Figures 2 and S7 and Table S2). In contrast, activity remained higher in the liver and kidney, with slower clearance from these tissues over time. From 1-24 h, activity in the liver fell by 52%, while 68% of the 1 h activity was excreted from the kidney by the end of the study. In addition, although appreciable accumulation ( $3.72 \pm 0.5\%$  ID/g) of activity in the tumor was observed at 1 h, it decreased by 54% at 24 h post-injection (p.i.). This yielded average tumor:blood and tumor:muscle ratios of 12, 95 and 42, and 2.4, 5.7 and 3.6 at 1, 4 and 24 h, respectively.

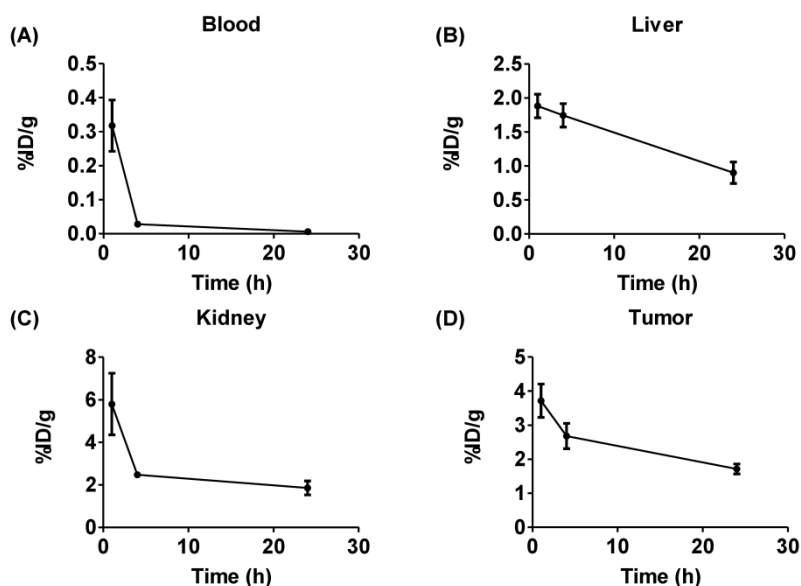


**Figure 2. Biodistribution of  $^{225}\text{Ac}$ -DOTA-c(RGDyK).** The radiotracer was injected into U87MG tumor bearing nude mice ( $n = 6$ /time point). While the radiotracer clears efficiently from the blood (A), clearance from the liver (B) and kidney (C) are more modest over time. (D) Tumor uptake is also relatively high.

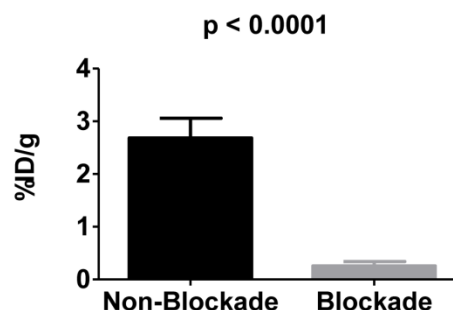


**Figure 3. In vivo blockade demonstrates specific targeting of  $\alpha_v\beta_3$  integrin.**  $\alpha_v\beta_3^+$  tumors demonstrate significantly more uptake of  $^{225}\text{Ac}$ -DOTA-c(RGDyK) when compared to  $\alpha_v\beta_3^+$  tumors in animals receiving the radiotracer and excess c(RGDyK) as blockade.

To examine the *in vivo* specificity of  $^{225}\text{Ac}$ -DOTA-c(RGDyK) for the receptor, blocking studies were performed at 4 h p.i. by co-injecting excess c(RGDyK) along with the analogous radiotracer (Figure 3). Injection of c(RGDyK) reduced accumulation of  $^{225}\text{Ac}$ -DOTA-c(RGDyK) in the tumor by 91% (non-block vs. block (%ID/g):  $2.68 \pm 0.037$  vs.  $0.26 \pm 0.085$ ;  $p < 0.0001$ ), suggesting that the radiopharmaceutical is being retained at the tumor site through specific interactions between the targeting RGD ligand and the  $\alpha_v\beta_3$  integrin. These results are in excellent agreement with previously published data that describe the biodistribution of analogous PET and SPECT radiopharmaceuticals designed to target this integrin [45, 50]. Furthermore, it suggests that the conjugation of the radiometal chelate did not interfere with ligand:receptor interactions, as predicted by our SPR experiments using La-DOTA-c(RGDyK).

Cerenkov luminescence imaging continues to evolve as an optical imaging technique with potential applications in preclinical drug development, radiopharmaceutical development, and surgical sciences by enhancing intraoperative techniques [16]. Only a few reports have described CLI in the context of the  $\alpha$ -emitting isotope  $^{225}\text{Ac}$ , which does not demonstrate prompt Cerenkov emissions, but relies upon the beta decay of  $^{213}\text{Bi}$ ,  $^{209}\text{Tl}$  and  $^{209}\text{Pb}$  to generate the optical signal that is detected using standard optical instrumentation [15, 19, 20]. Initial reports using *in silico* modeling and *in vitro* experimentation described a mandatory data acquisition delay of 10 hours for  $^{225}\text{Ac}$  to achieve equilibrium with its daughter radionuclides so that the measured light output in a unit volume would be proportional to the

activity of Ac-225 in that unit volume [19, 20]. With this criterion in mind, we injected U87mg tumor-bearing mice, with  $^{225}\text{Ac}$ -DOTA-c(RGDyK) or with  $^{225}\text{Ac}$ -DOTA-c(RGDyK) and excess c(RGDyK) as a blockade (Figure 4). We relied on the well-documented ability of RGD-containing ligands to be internalized on integrin binding to sequester the  $^{225}\text{Ac}$  and the daughter products within the tumor. Although not used as part of an imaging strategy, this technique, often referred to as the nanogenerator approach, has been used successfully to sequester  $^{225}\text{Ac}$ -based radiotherapeutics and daughter decay products within a cell to increase their therapeutic effectiveness [51-53]. Surprisingly, all animals tolerated  $^{225}\text{Ac}$ -DOTA-c(RGDyK) extremely well, demonstrating no signs of distress during these experiments. Twenty-four hours after radiopharmaceutical injection, whole-animal CLI revealed Cerenkov radiation emissions from the subcutaneous,  $\alpha_v\beta_3^+$  tumors and the liver and kidneys, which have been shown in related biodistribution studies to be involved in the clearance and excretion of this radiopharmaceutical [46, 54, 55]. *In vivo* imaging and ROI analysis (Figure 4A-C) revealed that tumors demonstrated an average

radiance of  $5.8 \times 10^3 \pm 0.5 \times 10^3$  p/s/cm<sup>2</sup>/sr, while tumors of animals receiving  $^{225}\text{Ac}$ -DOTA-c(RGDyK) and blockade demonstrated a significant reduction in average radiance ( $1.1 \times 10^3 \pm 0.08 \times 10^3$  p/s/cm<sup>2</sup>/sr;  $p < 0.0001$ ). These results suggest that activity delivered by the radiopharmaceutical and internalized through specific receptor-interactions is being retained in the tumor. Our data agree well with the biodistribution and blocking data reported for similar RGD systems radiolabeled with PET and SPECT isotopes [21, 50].

On *ex vivo* imaging (Figure S8 and Figure 4D), tumors had an average radiance of  $8.8 \times 10^3 \pm 1.6 \times 10^3$  p/s/cm<sup>2</sup>/sr; tumors of animals receiving the radiopharmaceutical and blockade demonstrated significantly less Cerenkov emission, with an average radiance of  $1.1 \times 10^3 \pm 0.25 \times 10^3$  p/s/cm<sup>2</sup>/sr ( $p < 0.0001$ ). All other tissues examined did not demonstrate significant Cerenkov emission. These results contrast with the biodistribution results that show some radioactivity retention in all tissues. This difference may be attributed to the volume-dependent nature of Cerenkov emissions within tissues of different sizes, and the differences in detection sensitivity between the optical imaging and gamma counting techniques employed in these studies.

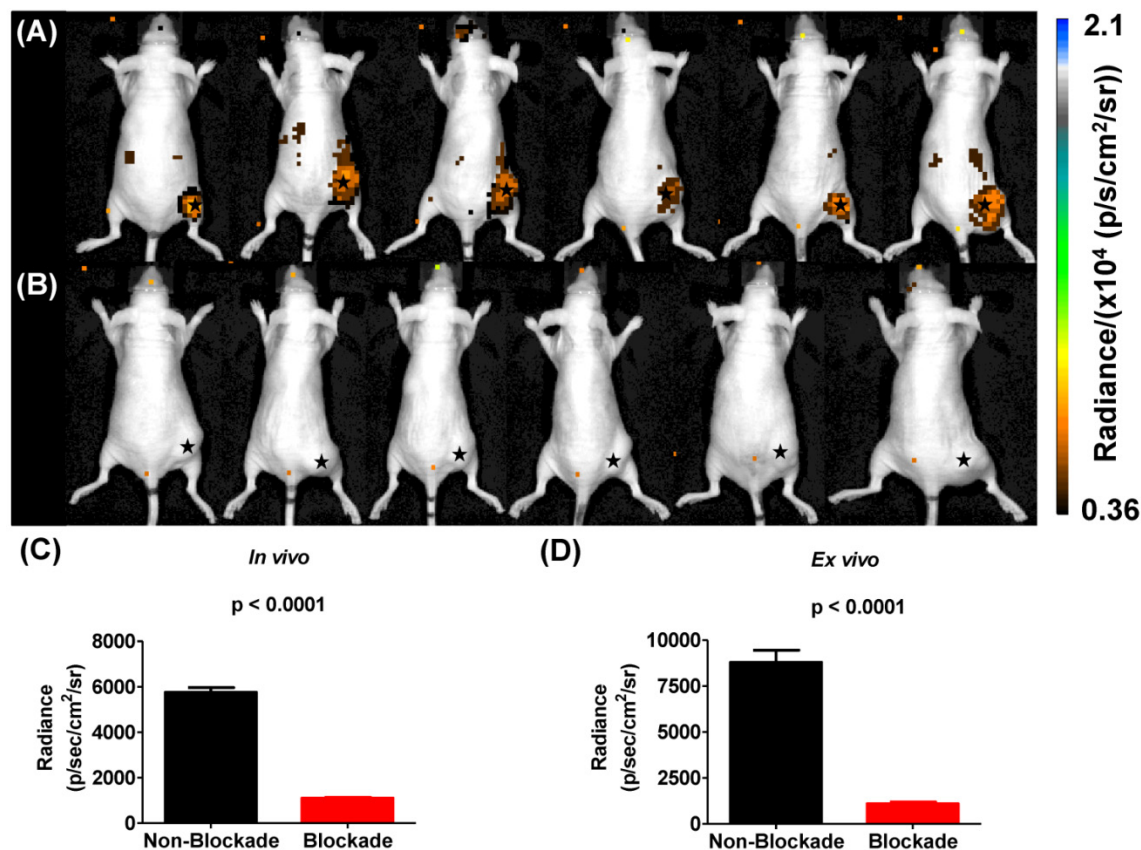


**Figure 4.** Cerenkov luminescence imaging with  $^{225}\text{Ac}$ -DOTA-c(RGDyK). Images were acquired 24 h after intravenous injection to allow for equilibrium to occur between  $^{225}\text{Ac}$  and its daughter products, which generate Cerenkov luminescence. (A) Efficient tumor localization was observed in U87mg tumor bearing animals at 24 h p.i. (B) Localization was reduced upon administration of blockade demonstrating *in vivo* specificity. (C, D) *In vivo* (C) and *ex vivo* (D) quantification based upon ROI analysis demonstrates that Cerenkov radiation in the tumor is significantly reduced upon the administration of blockade. (★) denotes tumor.

Based upon the results extrapolated from biodistribution data (Table S3), tumor clearance of radioactivity was approximately 3 fold slower than the clearance of radioactivity from the kidney. However, both tissues received a similar dose, which was not predicted by the CLI results. This finding corroborates an earlier publication that reported a similar observation in a murine model of leukemia [56].

We also completed preliminary therapy studies with  $^{225}\text{Ac}$ -DOTA-c(RGDyK) to further assess the theranostic potential of our approach (see Figure S9). Toxicity studies were completed in normal mice in order to determine the maximum tolerated dose of  $^{225}\text{Ac}$ -DOTA-c(RGDyK). By the end of the 16 week study, none of the animals achieved any of the predefined study endpoints, which included distressed behavior or average group weight loss of 15%, and only the cohort receiving the highest dose (0.16 MBq) demonstrated an average weight loss of  $10\pm 4\%$  compared to control animals. Nephrotoxicity is a well-documented consequence of targeted alpha particle therapy; thus, we measured blood urea nitrogen (BUN) and creatinine content in serum, as indicators of renal health [57, 58]. BUN retention was elevated in all cohorts compared to the control animals suggesting impairment. However, inter-individual values were high among all groups, so that the differences were not statistically significant (Figure S9C). We also measured serum levels of creatinine, a byproduct of muscle metabolism eliminated from the blood by glomerular filtration and proximal tubular secretion. Compared to the control cohort, creatinine levels were elevated in all groups that received doses of  $^{225}\text{Ac}$ -DOTA-c(RGDyK) above 0.04 MBq. In contrast to the BUN results, inter-individual values were not as divergent; suggesting that elevated levels of creatinine in serum could reflect real kidney damage and a true reduction in kidney function (Figure S9A). Finally, histopathologic examination indicated that only the cohorts receiving the two highest doses developed multi-focal tubular nephrosis with lymphocytic infiltration, consistent with radiation-induced damage to the tubular epithelium (Figure S10). All other cohorts did not exhibit pathological changes consistent with acute kidney damage or impaired renal function. Furthermore, liver pathology was normal among all cohorts despite the enhanced retention of the radiotracer. All other tissues were similar in treatment versus control groups, consistent with findings of other groups investigating  $^{225}\text{Ac}$ -labeled peptides for TAT [31].

Overall, we established the MTD of  $^{225}\text{Ac}$ -DOTA-c(RGDyK) to be 0.04 MBq, and initiated

therapy studies using female nude mice inoculated with human U87mg cells in the flank. Four days after inoculation, we randomly divided the mice into cohorts and treated them with saline, DOTA-c(RGDyK) or  $^{225}\text{Ac}$ -DOTA-c(RGDyK) at 0.04 MBq (1 MTD), 0.02 MBq (0.5 MTD) or 0.01 MBq (0.25 MTD). We then monitored tumor growth for 14 days after treatment to assess tumor burden. Based upon our results, a statistically significant reduction in tumor volume was achieved in animals receiving radiotherapy (Figure S9D). This suggests that tumor growth control can be achieved using doses of  $^{225}\text{Ac}$ -DOTA-c(RGDyK), which do not cause toxicity in non-target tissues. Furthermore, this growth control is observed with much lower levels of radioactivity than would be needed with  $\beta$  emitting radiopharmaceuticals that target the same integrin [50], and illustrates the cytotoxic potency of  $\alpha$ -emitting radiotherapeutics.

This report demonstrates through proof-of-concept studies that the secular equilibrium that exists between  $^{225}\text{Ac}$  and its daughter products can be used for *in vivo* tumor detection. Additionally, we provide data illustrating the low toxicity of  $^{225}\text{Ac}$ -DOTA-c(RGDyK) in normal mice and its ability to retard tumor growth compared to controls. Our findings suggest that  $^{225}\text{Ac}$ -based radiopharmaceuticals have theranostic potential that should be explored pre-clinically for translation into the clinic. However, several limitations of these studies should be considered [19, 20].

Although CLI is demonstrated here using an  $^{225}\text{Ac}$ -based radiopharmaceutical, not all  $\alpha$ -emitting radioisotopes will produce sufficient Cerenkov radiation to be useful for imaging. Secondly, given the 10 h time delay needed for equilibrium to be established between  $^{225}\text{Ac}$  and its daughter products, imaging the pharmacokinetics of small molecules and peptides at early time points is currently not possible. However, using this technique to monitor the biodistribution of  $^{225}\text{Ac}$ -labeled antibodies and nanoparticles, which require extended circulation time for effective tumor targeting and blood clearance, remains a possibility and worthy of exploration. Finally, the high recoil energy associated with  $^{225}\text{Ac}$  and daughter product release from the original conjugate must be considered. Emission of Cerenkov radiation may not reflect the actual biodistribution of the radiopharmaceutical in question, but of the daughter products producing the Cerenkov emissions [59]. We utilized a thoroughly established murine model and relied upon the nanogenerator approach to keep  $^{225}\text{Ac}$ -DOTA-c(RGDyK) and its daughter products within tumor cells. However, inability to retain every daughter

product after injection highlights the need for new materials, techniques, and mechanisms to effectively sequester the daughter products with the original conjugate to minimize the effects of this recoil energy. Several of these materials (including liposomes and  $\text{LaPO}_4$  based nanoparticles) have been described, and appear moderately effective in this arena [13, 60-64].

Preliminary toxicity and therapy studies demonstrated that low doses of  $^{225}\text{Ac}$ -DOTA-c(RGDyK) retarded tumor growth in mice 14 days after treatment. The potential of treating  $\alpha_v\beta_3^+$  tumors with  $^{225}\text{Ac}$ -RGD-based therapies remains unknown, since larger studies are needed.  $\alpha_v\beta_3^+$  malignancies demonstrate a diverse biology; understanding the effectiveness of these therapies among different cancer types will need to be elucidated [65]. Secondly, numerous reports have indicated that RGD multimerization increases tumor retention of several radiopharmaceuticals [54, 66-71];  $^{225}\text{Ac}$ -radiopharmaceuticals containing RGD monomers and multimers will need to be compared in the TAT setting. Finally, the use of these radiopharmaceuticals with other therapies or technologies such as pulsed high intensity focused ultrasound may enhance uptake and retention of this therapeutic in tumors [72-74]. This is a future direction to explore so that the maximum clinical benefit of this technology can be achieved.

While renal impairment was only observed in animals receiving the highest doses of  $^{225}\text{Ac}$ -DOTA-c(RGDyK), we did not conduct long-term toxicity studies. In earlier work that described  $^{212/213}\text{Bi}$ -based radiopharmaceuticals, late-onset nephrotoxicity was observed in mice [75-77]. Diminished renal function is one of the most critical factors hindering TAT therapy development and its clinical implementation. With respect to  $^{225}\text{Ac}$ -radiotherapeutics, the damage caused by radiotracer reabsorption in the proximal tubules or by the localization of  $^{213}\text{Bi}$  and  $^{221}\text{Fr}$  daughter products in the renal tubule cells needs to be addressed, since damage caused by these daughter products can lead to nephropathy and ultimately, renal failure. Several strategies have been proffered to minimize kidney toxicity [57, 58]. These include amino acid co-infusion to block peptide reabsorption; angiotensin 1 blockade; chelation therapy to sequester  $^{225}\text{Ac}$  daughter products; and diuresis using spironolactone, furosemide or chlorothiazide. However, the choice of remediation and its efficiency will depend on the therapeutic under investigation [48].

In summary, this communication describes the evaluation of  $^{225}\text{Ac}$ -DOTA-c(RGDyK) in both biodistribution and Cerenkov luminescence imaging studies. This radiopharmaceutical was prepared in excellent radiochemical purity and specific activity

that is in agreement with other  $^{225}\text{Ac}$ -based radiopharmaceuticals. It was highly stable *in vitro* and *in vivo* biodistribution studies confirmed the ability of the radiotracer to target  $\alpha_v\beta_3$  integrin with specificity. Our results confirm earlier reports that CLI with certain  $\alpha$ -emitting radiopharmaceuticals is possible in live animals as predicted by their theoretical and *in vitro* experiments [19, 20]. Furthermore, this concept may have broader implications for promising technological advancements in radiochemistry, radiopharmaceutical development, molecular imaging and the material sciences, and is worthy of further study. To our knowledge, this report is the first to describe Cerenkov luminescence imaging of  $\alpha_v\beta_3^+$  tumors in live animals using the *in situ* decay of  $^{225}\text{Ac}$  and its daughter products. This work could provide new ways in which to further enhance targeted alpha particle therapy.

## Supplementary Material

Supplementary schemes, figures and tables.  
<http://www.thno.org/v06p0698s1.pdf>

## Abbreviations

CLI: Cerenkov Luminescence Imaging; ESI-MS: Electrospray Ionization Mass Spectrometry; HBS: HEPES Buffered Saline; ITLC: Instant Thin Layer Chromatography; kBq: Kilobecquerel; K<sub>i</sub>: Inhibitory Constant; IC<sub>50</sub>: Half Maximal Inhibitory Concentration; MBq: Megabecquerel; %ID/g: Percent Injected Dose Per Gram of Tissue; P.I.: Post-injection; ROI: Region of Interest; RU: Response Unit; SPR: Surface Plasmon Resonance; TAT: Targeted Alpha Particle Therapy; TLC: Thin Layer Chromatography

## Acknowledgements

The isotope(s) used in this research were supplied by the United States Department of Energy Office of Science by the Isotope Program in the Office of Nuclear Physics. U87 mg cell culture was provided through the Cell Viral and Vector Core Laboratory, which is supported by the Wake Forest Comprehensive Cancer Center under the auspices of NIH grant P30 CA012197. Tissue histology was provided through the Comparative Pathology Laboratory, which is supported by the Wake Forest Comprehensive Cancer Center under the auspices of NIH grant P30 CA012197. The authors would like to thank Dr. Michael McDevitt of Memorial Sloan Kettering Cancer Center, New York, NY and Dr. Alfred Morgenstern of the Nuclear Chemistry Division, Institute of Transuranium Elements, Karlsruhe, DE for insightful comments and valuable discussions regarding this research.

## Grant support

NIH P30 CA012197 (WFUHS and TJW); DoD grant W81XWH-13-1-0125 (TJW); American Cancer Society grant 124443-MRSG-13-121-01-CDD (AM).

## Competing Interests

The authors have declared that no competing interest exists.

## References

- Wadas TJ, Pandya DN, Solingapuram Sai KK, Mintz A. Molecular targeted alpha-particle therapy for oncologic applications. *AJR Am J Roentgenol.* 2014; 203: 253-60.
- Scheinberg DA, McDevitt MR. Actinium-225 in targeted alpha-particle therapeutic applications. *Curr Radiopharm.* 2011; 4: 306-20.
- Wilbur DS. Chemical and radiochemical considerations in radiolabeling with alpha-emitting radionuclides. *Curr Radiopharm.* 2011; 4: 214-47.
- Kassis AI. Therapeutic radionuclides: biophysical and radiobiologic principles. *Semin Nucl Med.* 2008; 38: 358-66.
- Baidoo KE, Yong K, Brechbiel MW. Molecular pathways: targeted alpha-particle radiation therapy. *Clin Cancer Res.* 2013; 19: 530-537.
- Larson SM, Carrasquillo JA, Cheung NK, Press OW. Radioimmunotherapy of human tumours. *Nat Rev Cancer.* 2015; 15: 347-360.
- Jurcic JG, Rosenblat TL. Targeted alpha-particle immunotherapy for acute myeloid leukemia. *Am Soc Clin Oncol Educ Book.* 2014: e126-131.
- Morgenstern A, Bruchertseifer F, Apostolidis C. Bismuth-213 and actinium-225 -- generator alpha therapy: evidence for potential applications of two generator-derived alpha-emitting radioisotopes. *Curr Radiopharm.* 2012; 5: 221-227.
- Miederer M, Scheinberg DA, McDevitt MR. Realizing the potential of the Actinium-225 radionuclide generator in targeted alpha particle therapy applications. *Adv Drug Deliv Rev.* 2008; 60: 1371-1382.
- Couturier O, Supiot S, Degraef-Mougin M, Faivre-Chauvet A, Carlier T, Chatal JF, Davodeau F, Cherel M. Cancer radioimmunotherapy with alpha-emitting nuclides. *Eur J Nucl Med Mol Imaging.* 2005; 32: 601-614.
- Allen BJ. Targeted alpha therapy: evidence for potential efficacy of alpha-immunoconjugates in the management of micrometastatic cancer. *Australas Radiol.* 1999; 43: 480-486.
- McDevitt MR, Finn RD, Ma D, Larson SM, Scheinberg DA. Preparation of alpha-emitting <sup>213</sup>Bi-labeled antibody constructs for clinical use. *J Nucl Med.* 1999; 40: 1722-1727.
- McLaughlin MF, Robertson D, Pevsner PH, Wall JS, Mirzadeh S, Kennel SJ. LnPO<sub>4</sub> nanoparticles doped with Ac-225 and sequestered daughters for targeted alpha therapy. *Cancer Biother Radiopharm.* 2014; 29: 34-41.
- Lohrmann C, Zhang H, Thorek DL, Desai P, Zanzonico PB, O'Donoghue J, Irwin CP, Reiner T, Grimm J, Weber WA. Cerenkov luminescence imaging for radiation dose calculation of a <sup>90</sup>Y-labeled gastrin-releasing peptide receptor antagonist. *J Nucl Med.* 2015; 56: 805-811.
- Ruggiero A, Holland JP, Lewis JS, Grimm J. Cerenkov luminescence imaging of medical isotopes. *J Nucl Med.* 2010; 51: 1123-1130.
- Das S, Thorek DL, Grimm J. Cerenkov imaging. *Adv Cancer Res.* 2014; 124: 213-234.
- Thorek D, Robertson R, Bacchus WA, Hahn J, Rothberg J, Beattie BJ, Grimm J. Cerenkov imaging - a new modality for molecular imaging. *Am J Nucl Med Mol Imaging.* 2012; 2: 163-173.
- Thorek DL, Riedl CC, Grimm J. Clinical Cerenkov luminescence imaging of (18)F-FDG. *J Nucl Med.* 2014; 55: 95-98.
- Beattie BJ, Thorek DL, Schmidlein CR, Pentlow KS, Humm JL, Hielscher AH. Quantitative modeling of Cerenkov light production efficiency from medical radionuclides. *PLoS One.* 2012; 7: e31402-e31415.
- Ackerman NL, Graves EE. The potential for Cerenkov luminescence imaging of alpha-emitting radionuclides. *Phys Med Biol.* 2012; 57: 771-783.
- Liu Z, Wang F, Chen X. Integrin targeted delivery of radiotherapeutics. *Theranostics.* 2011; 1: 201-210.
- Niu G, Chen X. Why integrin as a primary target for imaging and therapy. *Theranostics.* 2011; 1: 30-47.
- Deal KA, Davis IA, Mirzadeh S, Kennel SJ, Brechbiel MW. Improved in vivo stability of actinium-225 macrocyclic complexes. *J Med Chem.* 1999; 42: 2988-2992.
- Hantgan RR, Stahle MC, Horita DA. Entropy drives integrin alphaIIb beta3:echistatin binding--evidence from surface plasmon resonance spectroscopy. *Biochemistry.* 2008; 47: 2884-2892.
- Dutta S, Horita DA, Hantgan RR, Guthold M. Probing IIb3: Ligand interactions by dynamic force spectroscopy and surface plasmon resonance. *Nano Life.* 2013; 3: 13400051-134000511.
- Hantgan RR, Stahle MC, Lord ST. Dynamic regulation of fibrinogen: integrin alphaIIb beta3 binding. *Biochemistry.* 2010; 49: 9217-9225.
- Pandya DN, Pailloux S, Tatum D, Magda D, Wadas TJ. Di-macrocyclic terephthalamide ligands as chelators for the PET radionuclide zirconium-89. *Chem Commun.* 2015; 51: 2301-2303.
- Sgouros G, Roeske JC, McDevitt MR, Palm S, Allen BJ, Fisher DR, Brill AB, Song H, Howell RW, Akabani G, Bolch WE, Meredith RF, Wessels BW, Zanzonico PB. MIRD Pamphlet No. 22 (abridged): radiobiology and dosimetry of alpha-particle emitters for targeted radionuclide therapy. *J Nucl Med.* 2010; 51: 311-328.
- Radchenko V, Engle JW, Wilson JJ, Maassen JR, Nortier FM, Taylor WA, Birnbaum ER, Hudston LA, John KD, Fassbender ME. Application of ion exchange and extraction chromatography to the separation of actinium from proton-irradiated thorium metal for analytical purposes. *J Chromatogr A.* 2015; 1380: 55-63.
- Henkin R, Bova D, Dillehay G, Karesh S, Halama J, Wagner R, Zimmer A. *Nuclear Medicine.* 2 ed. St. Louis: Mosby-Year Books; 1996.
- Miederer M, Henriksen G, Alke A, Mossbrugger I, Quintanilla-Martinez L, Senekowitsch-Schmidtko R, Essler M. Preclinical evaluation of the alpha-particle generator nuclide <sup>225</sup>Ac for somatostatin receptor radiotherapy of neuroendocrine tumors. *Clin Cancer Res.* 2008; 14: 3555-3561.
- Kirby H, Morss L. Actinium. Amsterdam: Springer; 2006.
- Edelstein N, Fuger J, Katz J, Morss L. *The Chemistry of the Actinide and Transactinide Elements.* Amsterdam: Springer; 2006.
- Teixeira JM, Dias DM, Canada FJ, Martins JA, Andre JP, Jimenez-Barbero J, Geraldes CF. The interaction of La(3+) complexes of DOTA/DTPA glycoconjugates with the RCA(120) lectin: a saturation transfer difference NMR spectroscopic study. *J Biol Inorg Chem.* 2011; 16: 725-734.
- McDonnell JM. Surface plasmon resonance: towards an understanding of the mechanisms of biological molecular recognition. *Curr Opin Chem Biol.* 2001; 5: 572-577.
- Schuck P. Use of surface plasmon resonance to probe the equilibrium and dynamic aspects of interactions between biological macromolecules. *Annu Rev Biophys Biomol Struct.* 1997; 26: 541-566.
- Guo X. Surface plasmon resonance based biosensor technique: a review. *J Biophotonics.* 2012; 5: 483-501.
- Rocco M, Rosano C, Weisel JW, Horita DA, Hantgan RR. Integrin conformational regulation: uncoupling extension/tail separation from changes in the head region by a multiresolution approach. *Structure.* 2008; 16: 954-964.
- Arnaout MA, Mahalingam B, Xiong JP. Integrin structure, allostery, and bidirectional signaling. *Annu Rev Cell Dev Biol.* 2005; 21: 381-410.
- Dong X, Mi LZ, Zhu J, Wang W, Hu P, Luo BH, Springer TA. alpha(V)beta(3) integrin crystal structures and their functional implications. *Biochemistry.* 2012; 51: 8814-8828.
- Takagi J, Petre BM, Walz T, Springer TA. Global conformational rearrangements in integrin extracellular domains in outside-in and inside-out signaling. *Cell.* 2002; 110: 599-611.
- Xiong JP, Stehle T, Zhang R, Joachimiak A, Frech M, Goodman SL, Arnaout MA. Crystal structure of the extracellular segment of integrin alpha Vbeta3 in complex with an Arg-Gly-Asp ligand. *Science.* 2002; 296: 151-155.
- Hancock MA, Spencer CA, Koschinsky ML. Definition of the structural elements in plasminogen required for high-affinity binding to apolipoprotein(a): a study utilizing surface plasmon resonance. *Biochemistry.* 2004; 43: 12237-12248.
- Hojo E, Watanabe K, Tsukamoto T. Real-time kinetic analyses of the interaction of ricin toxin A-chain with ribosomes prove a conformational change involved in complex formation. *J Biochem.* 2002; 131: 267-275.
- Jeong JM, Hong MK, Chang YS, Lee YS, Kim YJ, Cheon GJ, Lee DS, Chung JK, Lee MC. Preparation of a promising angiogenesis PET imaging agent: <sup>68</sup>Ga-labeled c(RGDyK)-isothiocyanatobenzyl-1,4,7-triazacyclononane-1,4,7-triacetic acid and feasibility studies in mice. *J Nucl Med.* 2008; 49: 830-836.
- Chen X, Hou Y, Tohme M, Park R, Khankaldyyan V, Gonzales-Gomez I, Bading JR, Laug WE, Conti PS. Pegylated Arg-Gly-Asp peptide: <sup>64</sup>Cu labeling and PET imaging of brain tumor alphavbeta3-integrin expression. *J Nucl Med.* 2004; 45: 1776-1783.
- Essler M, Gartner FC, Neff F, Blechert B, Senekowitsch-Schmidtko R, Bruchertseifer F, Morgenstern A, Seidl C. Therapeutic efficacy and toxicity of <sup>225</sup>Ac-labelled vs. <sup>213</sup>Bi-labelled tumour-homing peptides in a preclinical mouse model of peritoneal carcinomatosis. *Eur J Nucl Med Mol Imaging.* 2012; 39: 602-612.
- Song H, Hobbs RF, Vajravelu R, Huso DL, Esaias C, Apostolidis C, Morgenstern A, Sgouros G. Radioimmunotherapy of breast cancer metastases with alpha-particle emitter <sup>225</sup>Ac: comparing efficacy with <sup>213</sup>Bi and <sup>90</sup>Y. *Cancer Res.* 2009; 69: 8941-8948.
- Antczak C, Jaggi JS, LeFave CV, Curcio MJ, McDevitt MR, Scheinberg DA. Influence of the linker on the biodistribution and catabolism of actinium-225 self-immolative tumor-targeted isotope generators. *Bioconjug Chem.* 2006; 17: 1551-1560.
- Chen X. Integrin Targeted Imaging and Therapy. *Theranostics.* 2011; 2011: 28-29.
- McDevitt MR, Ma D, Lai LT, Simon J, Borchardt P, Frank RK, Wu K, Pellegrini V, Curcio MJ, Miederer M, Bander NH, Scheinberg DA. Tumor therapy with targeted atomic nanogenerators. *Science.* 2001; 294: 1537-1540.
- Miederer M, McDevitt MR, Borchardt P, Bergman I, Kramer K, Cheung NK, Scheinberg DA. Treatment of neuroblastoma meningeal carcinomatosis with

- intrathecal application of alpha-emitting atomic nanogenerators targeting disialo-ganglioside GD2. *Clin Cancer Res.* 2004; 10: 6985-6992.
53. Miederer M, McDevitt MR, Sgouros G, Kramer K, Cheung NK, Scheinberg DA. Pharmacokinetics, dosimetry, and toxicity of the targetable atomic generator,  $^{225}\text{Ac}$ -HuM195, in nonhuman primates. *J Nucl Med.* 2004; 45: 129-137.
54. Chen X, Liu S, Hou Y, Tohme M, Park R, Bading JR, Conti PS. MicroPET imaging of breast cancer alphav-integrin expression with  $^{64}\text{Cu}$ -labeled dimeric RGD peptides. *Mol Imaging Biol.* 2004; 6: 350-359.
55. Chen X, Park R, Tohme M, Shahinian AH, Bading JR, Conti PS. MicroPET and autoradiographic imaging of breast cancer alpha v-integrin expression using  $^{18}\text{F}$ - and  $^{64}\text{Cu}$ -labeled RGD peptide. *Bioconjug Chem.* 2004; 15: 41-49.
56. Balkin ER, Kenoyer A, Orozco JJ, Hernandez A, Shadman M, Fisher DR, Green DJ, Hyilarides MD, Press OW, Wilbur DS, Pagel JM. In vivo localization of (9)(0)Y and (1)(7)(7)Lu radioimmunoconjugates using Cerenkov luminescence imaging in a disseminated murine leukemia model. *Cancer Res.* 2014; 74: 5846-5854.
57. Jaggi JS, Seshan SV, McDevitt MR, LaPerle K, Sgouros G, Scheinberg DA. Renal tubulointerstitial changes after internal irradiation with alpha-particle-emitting actinium daughters. *J Am Soc Nephrol.* 2005; 16: 2677-26789.
58. Jaggi JS, Seshan SV, McDevitt MR, Sgouros G, Hyjek E, Scheinberg DA. Mitigation of radiation nephropathy after internal alpha-particle irradiation of kidneys. *Int J Radiat Oncol Biol Phys.* 2006; 64: 1503-1512.
59. Sgouros G. Long-lived alpha emitters in radioimmunotherapy: the mischievous progeny. *Cancer Biother Radiopharm.* 2000; 15: 219-221.
60. Henriksen G, Schoultz BW, Michaelsen TE, Bruland OS, Larsen RH. Sterically stabilized liposomes as a carrier for alpha-emitting radium and actinium radionuclides. *Nucl Med Biol.* 2004; 31: 441-449.
61. Jaggi JS, Kappel BJ, McDevitt MR, Sgouros G, Flombaum CD, Cabassa C, Scheinberg DA. Efforts to control the errant products of a targeted in vivo generator. *Cancer Res.* 2005; 65: 4888-4895.
62. Sofou S, Kappel BJ, Jaggi JS, McDevitt MR, Scheinberg DA, Sgouros G. Enhanced retention of the alpha-particle-emitting daughters of Actinium-225 by liposome carriers. *Bioconjug Chem.* 2007; 18: 2061-2067.
63. Sofou S, Thomas JL, Lin HY, McDevitt MR, Scheinberg DA, Sgouros G. Engineered liposomes for potential alpha-particle therapy of metastatic cancer. *J Nucl Med.* 2004; 45: 253-260.
64. Woodward J, Kennel SJ, Stuckey A, Osborne D, Wall J, Rondinone AJ, Standaert RF, Mirzadeh S.  $\text{LaPO}_4$  nanoparticles doped with actinium-225 that partially sequester daughter radionuclides. *Bioconjug Chem.* 2011; 22: 766-776.
65. Stupack DG. The biology of integrins. *Oncology (Williston Park).* 2007; 21: 6-12.
66. Chen X, Plasencia C, Hou Y, Neamati N. Synthesis and biological evaluation of dimeric RGD peptide-paclitaxel conjugate as a model for integrin-targeted drug delivery. *J Med Chem.* 2005; 48: 1098-1106.
67. Chen X, Tohme M, Park R, Hou Y, Bading JR, Conti PS. Micro-PET imaging of alphavbeta3-integrin expression with  $^{18}\text{F}$ -labeled dimeric RGD peptide. *Mol Imaging.* 2004; 3: 96-104.
68. Chin FT, Shen B, Liu S, Berganos RA, Chang E, Mitra E, Chen X, Gambhir SS. First experience with clinical-grade ( $^{18}\text{F}$ )FPP(RGD(2)): an automated multi-step radiosynthesis for clinical PET studies. *Mol Imaging Biol.* 2012; 14: 88-95.
69. Guo N, Lang L, Li W, Kiesewetter DO, Gao H, Niu G, Xie Q, Chen X. Quantitative analysis and comparison study of [ $^{18}\text{F}$ ]AIF-NOTA-PRGD2, [ $^{18}\text{F}$ ]FPPRGD2 and [ $^{68}\text{Ga}$ ]Ga-NOTA-PRGD2 using a reference tissue model. *PLoS One.* 2012; 7: e37506-e37515.
70. Lang L, Li W, Guo N, Ma Y, Zhu L, Kiesewetter DO, Shen B, Niu G, Chen X. Comparison study of [ $^{18}\text{F}$ ]FAL-NOTA-PRGD2, [ $^{18}\text{F}$ ]FPPRGD2, and [ $^{68}\text{Ga}$ ]Ga-NOTA-PRGD2 for PET imaging of U87MG tumors in mice. *Bioconjug Chem.* 2011; 22: 2415-2422.
71. Liu Z, Liu S, Wang F, Chen X. Noninvasive imaging of tumor integrin expression using (18)F-labeled RGD dimer peptide with PEG (4) linkers. *Eur J Nucl Med Mol Imaging.* 2009; 36: 1296-1307.
72. Dromi S, Frenkel V, Luk A, Traugher B, Angstadt M, Bur M, Poff J, Xie J, Libutti SK, Li KC, Wood BJ. Pulsed-high intensity focused ultrasound and low temperature-sensitive liposomes for enhanced targeted drug delivery and antitumor effect. *Clin Cancer Res.* 2007; 13: 2722-2727.
73. Frenkel V, Li KC. Potential role of pulsed-high intensity focused ultrasound in gene therapy. *Future Oncol.* 2006; 2: 111-119.
74. Frenkel V, Etherington A, Greene M, Quijano J, Xie J, Hunter F, Dromi S, Li KC. Delivery of liposomal doxorubicin (Doxil) in a breast cancer tumor model: investigation of potential enhancement by pulsed-high intensity focused ultrasound exposure. *Acad Radiol.* 2006; 13: 469-479.
75. Kang CS, Song HA, Milenic DE, Baidoo KE, Brechbiel MW, Chong HS. Preclinical evaluation of NETA-based bifunctional ligand for radioimmunotherapy applications using  $^{212}\text{Bi}$  and  $^{213}\text{Bi}$ : radiolabeling, serum stability, and biodistribution and tumor uptake studies. *Nucl Med Biol.* 2013; 40: 600-605.
76. Song EY, Abbas Rizvi SM, Qu CF, Raja C, Brechbiel MW, Morgenstern A, Apostolidis C, Allen BJ. Pharmacokinetics and toxicity of (213)Bi-labeled PAI2 in preclinical targeted alpha therapy for cancer. *Cancer Biol Ther.* 2007; 6: 898-904.
77. Qu CF, Songl YJ, Rizvi SM, Li Y, Smith R, Perkins AC, Morgenstern A, Brechbiel M, Allen BJ. In vivo and in vitro inhibition of pancreatic cancer growth by targeted alpha therapy using  $^{213}\text{Bi}$ -CHX.A"-C595. *Cancer Biol Ther.* 2005; 4: 848-853.